Research Article

Hammad Alotaibi* and Khuram Rafique

Numerical simulation of nanofluid flow between two parallel disks using 3-stage Lobatto III-A formula

https://doi.org/10.1515/phys-2022-0059
received March 15, 2022; accepted June 09, 2022

Abstract: The development of nanofluid technology has become a key research area in physics, mathematics, engineering, and materials science. Nowadays, in many industrial applications, nanofluids are widely used to enhance thermophysical properties such as thermal diffusivity, thermal conductivity, and convective heat transfer. Scientists and engineers have established interests in the direction of flow problems developed *via* disk-shaped bodies. There are various logics to discuss flow phenomenon due to rotating bodies, but its applications include in thermal power engineering system, gas turbine rotors, air cleaning machines, aerodynamics, *etc*. Nowadays manufacturing industries have inaugurated to select liquid based on heat transfer properties. Therefore, this article focuses on studying the laminar incompressible nanofluid between two parallel disks. Mathematical formulations of the law of conservation of mass, momentum, and heat transfer are investigated numerically. By using suitable similarities, the flow equations are converted into nonlinear ordinary differential equations. The resulting equations were solved numerically *via* MATLAB software. The effects of physical parameters of interest, such as Reynolds number, magnetic factor, Brownian parameter, and thermophoresis parameter on normal velocity, streamwise velocity, temperature, and concentration profiles are computed and presented using the graphs. The results revealed that the energy profile significantly rises, and the profile moves closer to the upper disk by enhancing the Brownian motion and thermophoresis parameter. The dynamics behind this is that by increasing the Brownian motion, the boundary layer wideness increases which increases the temperature. Moreover, streamwise velocity increases for large values of Reynolds number. Besides, the thermophoresis profile increases for large values of the thermophoresis factor. It could be observed that shear stress at nonporous/porous disk is adjusted by selecting a suitable value of injection velocity at the porous disk. Also, normal velocity decreases by increasing the parameter M.

Keywords: 3-stage Lobatto III-A formula, nanofluid, permeable disk, numerical solution

Nomenclature

B_0	constant magnetic field
C	nanoparticle concentration
D_B	Brownian diffusion coefficient
D_T	thermophoresis diffusion coefficient
Le	Lewis number
M	Hartmann number
Nb	Brownian motion parameter
Nt	thermophoresis parameter
Pr	Prandtl number
p	pressure
R	Reynolds number
T_m	mean temperature of the fluid
T	temperature of the fluid
u	axial velocity component
ν	kinematic viscosity
v	constant suction/injection velocity
w	radial velocity component
ρ	fluid density
μ	dynamic viscosity
σ	Boltzmann constant

1 Introduction

In recent years, there has been a growing interest and substantial improvement in nanofluids due to their enormous

* **Corresponding author: Hammad Alotaibi,** Department of Mathematics and Statistics, College of Science, Taif University, P.O. Box 11099, Taif, 21944, Saudi Arabia, e-mail: hm.alotaibi@tu.edu.sa
Khuram Rafique: Department of Mathematics, University of Sialkot, Sialkot, 51040, Pakistan, e-mail: khurram.rafique1005@gmail.com

potential to enhance heat transfer which has vast applications in the field of biochemical, engineering, biomedical sciences, and industry. The word "nanofluid" alludes to a fluid interruption of tiny rigid atoms having dimensions regularly of 1–100 nm in a regular liquid. In the late 1995s, nanofluid was introduced by Choi and Eastman [1], and they checked that the thermal conductivity of the fluids upgrade by the incorporation of these nanoparticles in base fluids. To feature the immense impacts of thermophoretic as well as Brownian movement dissemination of nanoparticles, a scientific model was introduced by Buongiorno [2].

Numerous analysts utilized this model to dissect the movement of the Nanofluids in different geometries. Several methods have been previously proposed that aim to enhance the thermal conductivity. For example, Sheikholeslami *et al.* [3] discussed the study of natural convection heat exchange in a nanofluid-packed field with an elliptic internal cylinder. Dogonchi *et al.* [4] analyzed nanofluid flow between parallel disks by considering the heat flux model. Khan *et al.* [5] worked on the Nanofluid flow between two parallel plates and examined the heat and mass transfer effect. Sheikholeslami and Abelman [6] discussed the heat transfer for nanofluid flow numerically. Hosseinzadeh *et al.* [7] explained nanofluid fluid flow analytically between analogous sheets. Rafique *et al.* [8] examined the effects of thermophoresis and Brownian motion on nanofluid flow for a slanted plate. Noor *et al.* [9] presented mixed convection micropolar nanofluid flow toward a vertically enlarging surface. Mabood *et al.* [10] analyzed nanofluid boundary layer flow and heat transfer along with a nonlinearly stretching sheet.

The physics of energy transfer in rapidly moving machines and engines with lubricant insides is playing a very useful role in daily life. Therefore, it has been an active area of research these days which helps today's practical life. The study of the heat transfer phenomenon is necessary for these systems for consistent and safe working of such machines. Magnetohydrodynmaic (MHD) has attracted a lot of interest due to its variety of applications. Some noteworthy innovative uses of MHD are in tests of measured atomic combination where a magnetic field is utilized to restrict poles of sizzling plasma, to create energy where fluid metals are compelled over a magnetic field, *etc.* Besides, MHD standards are utilized for shuttle impetus and light-ion-beam-driven inertial constraint. Some amazing endeavors have been made to examine the impact of MHD on different flow conditions. The extensive literature on the MHD flows in the existence of applied magnetic fields occurs nowadays. Likewise, Azimi and Riazi [11] attempted analytical methods for solving MHD convective and slip flow due to a spinning disk. Makinde *et al.* [12] probed the flow over a disk by considering different nanoparticles. Turkyilmazoglu [13] discussed the particular result of MHD viscid fluid by a revolving disk. Furthermore, Rafique *et al.* [14] described the properties of energy and species exchange in MHD flow for slanted sheets. Rafique *et al.* [15] probed the MHD stream of nano liquid along with the slanted sheet. Recently, Iqbal *et al.* [16] considered a wavy stretchy surface for nanoliquid flow by incorporating magnetic impacts. Furthermore, Iqbal *et al.* [17] utilized hybrid nanoliquid for the stretchy wavy geometry by taking magnetic effect.

In the same vein, the fluid movement over parallel disks has picked up great significance because of its extensive variety of technical and industrial uses, for example, laptop packing devices, semiconductor engineering procedures, thrust bearings, air turbine motors, biomechanics, *etc.* Elcrat [18] initially demonstrated the hypothesis of the non-rotational liquid wave over settled permeable disks with constant subjective drag or injunction. Ibrahim [19] has examined viscid unstable flow among adjacent disks. Vajravelu *et al.* [20] have investigated the squeezing flow of nanoliquid and energy exchange rate through parallel disks. Moreover, Bhatta *et al.* [21] discussed nanofluid unsteady flow with slip impacts. Hayat *et al.* [22] discussed the energy exchange rate for nanofluid flow for disks. Recently, Mustafa extended the von Karman problem of the infinite rotating disk by using Buongiorno's model. Sobamowo *et al.* [23] discussed nanofluid flow between two corresponding disks. Recently, Ghaffari *et al.* [24] examined two stretchy disks for power law nanoliquid *via* shooting technique. They discussed energy exchange phenomenon. Aziz *et al.* [25] probed three-dimensional (3D) flow for nanofluid by rotating disk. Elakkiyapriya and Anjali [26] examined the nanofluid flow because of the spinning disk. Hatami *et al.* [27] investigated 3D nanofluid with the help of an analytical method. Yin *et al.* [28] discussed nanofluid with heat transfer over a disk. Rafique *et al.* [29] investigated energy and mass exchange *via* numerical simulation of nanofluid. Alotaibi *et al.* [30] treated Casson nanofluid numerically over a heated extended surface. For higher order chemical reactions with heat source (sink) impacts, Alotaibi and Eid [31] proposed a model to study the flow of Darcy–Forchheimer's 3D permeable nanofluid through convective heating of porous extended surfaces considering the effect of magnetic fields and nonlinear radiation. Furthermore, by using the Keller box technique following the finite difference method in the MATLAB program, Alotaibi and Rafique [32] investigated mixed convection heat and mass transfer

of non-homogenous nanofluid around a vertical Riga plate in the presence of MHD effect. Different researchers [33–36] contributed valuable research work in the latest research area by considering different fluid models.

Engineers and scientists aim to explore further investigations of flow characteristics between disks due to wide range of applications of such flow in different varieties of field such as lubrication, heat and mass exchange, biomechanics, rotating machinery, *etc*. To our knowledge, there is no investigation so far that has been devoted to study the proposed model for nanofluid between two parallel disks by incorporating Brownian movement and thermophoresis impacts. Therefore, the principle aim of this article is to present a sufficient understanding of the mechanism of heat transfer as well as mass exchange in nanofluids flow behavior through porous and non-porous parallel disks. Here we restrict attention to nanofluid flow over parallel disks by taking Brownian motion and thermophoresis effects to enhance the heat transfer performance of viscous fluid [37]. It is known that various methods are available for the numerical solution of the considered problem, but we employed the Lobatto formula for the solution. Because this method is built by finite difference technique in bvp4c *via* Matlab software. This method is very easy for the numerical solutions of complicated ordinary differential equations (ODEs) of flow problems. In addition, this research pays intention to the heat as well as mass transportation which is very helpful in industry, engineering viewpoint, and practical life *via* the hydraulic engine, generators, electric motors, *etc*. This work has potential application in the implications of many devices including electronics, air conditioning, power, and chemical. It is expected that the results recovered in this study will not only helpful to give the information about industrial and engineering uses but also compliment on the published work.

2 Problem formulation

This numerical investigation is conducted for nanofluids between two analogous disks. The higher disk is porous, while the other is nonporous. Furthermore, the flow of nanofluid is driven with a continuous pressure gradient having velocity U. The lower disk is located at $z = -L$ and the upper disk is at $z = L$ with center at $z = 0$ as shown in Figure 1.

The governing equations for the flow of nanofluids between parallel disks by following Ashraf and Wehgal are [37]:

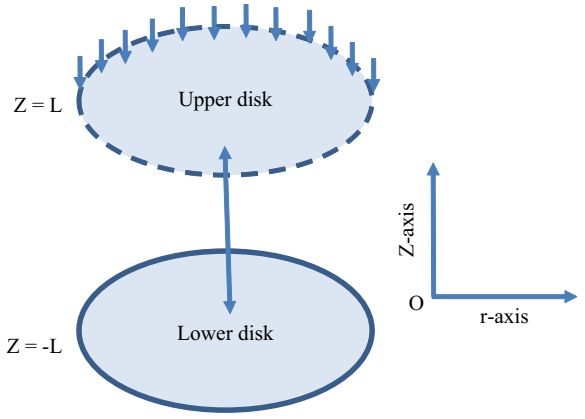

Figure 1: Physical sketch of the proposed problem.

$$\frac{\partial u}{\partial r} + \frac{u}{r} + \frac{\partial w}{\partial z} = o, \tag{1}$$

$$u\frac{\partial u}{\partial r} + w\frac{\partial u}{\partial z} = -\frac{1}{\delta_f}\frac{\partial p}{\partial r} + \vartheta\left(\frac{\partial^2 u}{\partial r^2} + \frac{\partial^2 u}{\partial z^2} + \frac{1}{r}\frac{\partial u}{\partial r} - \frac{u}{r^2}\right) - \frac{\sigma B_0^2}{\rho}u, \tag{2}$$

$$u\frac{\partial w}{\partial r} + w\frac{\partial w}{\partial z} = -\frac{1}{\delta_f}\frac{\partial p}{\partial r} + \vartheta\left(\frac{\partial^2 w}{\partial r^2} + \frac{\partial^2 w}{\partial z^2} + \frac{1}{r}\frac{\partial w}{\partial r}\right), \tag{3}$$

$$u\frac{\partial T}{\partial r} + w\frac{\partial T}{\partial z} = \alpha\left(\frac{\partial^2 T}{\partial r^2} + \frac{1}{r}\frac{\partial T}{\partial r} + \frac{\partial^2 T}{\partial z^2}\right) + \left[\tau\left(D_B\left(\frac{\partial c}{\partial r}\frac{\partial T}{\partial r} + \frac{\partial c}{\partial z}\frac{\partial T}{\partial z}\right) + \frac{D_t}{T_m}\left\{\left(\frac{\partial T}{\partial r}\right)^2 + \left(\frac{\partial T}{\partial z}\right)^2\right\}\right)\right], \tag{4}$$

$$u\frac{\partial c}{\partial r} + w\frac{\partial c}{\partial z} = D_B\left(\frac{\partial^2 c}{\partial r^2} + \frac{1}{r}\frac{\partial c}{\partial r} + \frac{\partial^2 c}{\partial z^2}\right) + \frac{D_t}{T_m}\left(\frac{\partial^2 T}{\partial r^2} + \frac{1}{r}\frac{\partial T}{\partial r} + \frac{\partial^2 T}{\partial z^2}\right). \tag{5}$$

The boundary settings for lower and upper disks by following Ashraf *et al.* [38] are given as

$$w(r, -L) = 0, \quad w(r, L) = 2v \qquad u(r, -L) = 0, \quad u(r, L) = 0. \tag{6}$$

where $2v$ denotes uniform and constant suction/injection velocity magnitude at the upper disk. Moreover, the lower disk is taken as nonporous. In view of Ashraf and Wehgal [37], the boundary settings for temperature and concentration are given as

$$T = T_1, \quad C = C_1 \text{ at } \eta = -1, \tag{7}$$
$$T = T_2, \quad C = C_2 \text{ at } \eta = 1.$$

Here we use the Von Karman [39] and Elko [40] similarity transformations to reduce the above partial equations into ordinary differential equations.

$$\psi(r, \eta) = \frac{vr^2}{2} f(\eta), \quad \theta = \frac{T - T_1}{T_2 - T_1}, \quad \varphi = \frac{c - c_1}{c_2 - c_1}. \tag{8}$$

by eliminating the pressure term, we get:

$$f^{iv} = \frac{2L}{\vartheta} ff''' + \frac{\sigma B_0^2}{\mu} L^2 f''. \tag{9}$$

By using the following dimensionless variables into Eq. (9):

$$f(\eta) = \frac{F(z)}{v}, \quad \text{where} \quad \eta = \frac{z}{L}.$$

Therefore, Eq. (9) becomes:

$$f^{iv} - 2Rff''' - M^2 f'' = 0. \tag{10}$$

Eqs. (4) and (5) become

$$\theta'' + \text{Pr} \quad \text{Nb}\theta'\varphi' + \text{PrNt}\theta'^2 - 2f\text{RPr}\theta' = 0, \tag{11}$$

$$\varnothing'' - 2f\text{RLe}\varnothing' + \left(\frac{\text{Nt}}{\text{Nb}}\right)\theta'' = 0, \tag{12}$$

where

$M = \frac{\sigma L B_0^2}{\mu}$, $R = \frac{\rho v L}{\mu}$ $\text{Pr} = \frac{\nu}{D_\text{B}}$, $\text{Le} = \frac{\nu}{\alpha}$,
$\text{Nb} = \frac{\tau D_\text{B}(c_w - c_h)}{\nu}$, and $\text{Nt} = \frac{\tau D_t (T_w - T_h)}{T_\text{m} \nu}$

With associate boundary conditions:

$$f(-1) = 0, f(1) = 1, \theta(-1) = 1, \theta(1) = 0, \tag{13}$$
$$f'(-1) = 0, f'(1) = 0, \varnothing(-1) = 1, \varnothing(1) = 0. \tag{14}$$

3 Numerical solution

In order to find the numerical solution of Eqs. (10)–(12) subject to the boundary conditions (13)–(14), we employ the Lobatto formula. This method can be depicted in MATLAB 2010 by a built-in function named "bvp4c." This is a finite difference method executed in three stage Lobatto III-A formula. This is also known *via* the collocation method with fourth-order accuracy. This numerical technique is very helpful to solve all kinds of complicated nonlinear ODE's. For this, we transform our governing nonlinear ODEs into a first-order ODEs system by introducing:

$$y_1 = f', \quad y_2 = f'', y_3 = f''', y_4 = \theta', y_5 = \phi'$$

Table 1: Values of the heat transfer rate $\theta'(-1)$ and mass transfer rate $\varnothing'(-1)$ for different values of Nb and Nt, when $M = 1$, $R = -10$, Le = 2

R	M	Le	Nb	Nt	$\theta'(-1)$	$\varnothing'(-1)$
−10	1.0	2	0.1	0.3	−1.829	−2.014
			0.5		−1.520	−3.051
			1		−1.193	−3.164
			1.5		−0.0928	−3.191
			2		−0.714	−3.197
			0.5	0	−1.664	−3.137
				0.1	−1.614	−3.096
				0.2	−1.566	−3.068
				0.3	−1.520	−3.051
				0.4	−1.475	−3.044

For "bvp4c" function, we use a routine named "NANO_ODE," which has the system of 1st order ODEs as mentioned above. "NANO_BC" is used for boundary conditions and "NANO_GUESS" is used for the initial guess which fulfilled our boundary conditions.

4 Results and discussion

This section contains the discussions and interpretations of our findings in graphical and tabular form. Numerous figures as well as tables are prepared for numerical interpretation. Table 1 exhibits the statistical results of $\theta'(-1)$ and $\phi'(-1)$. Table 1 elucidated the mathematical values of energy and species exchange at the bottom disk for the variation in Brownian motion and thermophoresis. In same vein from Table 1, we can perceive that the values of heat exchange growths for the values of Nb, and this due to the irregular movement of particles which causes the collisions between fluid particles in return kinetic energy boost up while, opposite in the case of the mass exchange rate. Furthermore, the values of $\theta'(-1)$ and $\varnothing'(-1)$ increase with the increase in the values of thermophoresis (Nt). Physically, it can be argued that boundary layer thickness enhances by increasing the strength of Nb. To check the validity of our solution, we compare Figures 2 and 3 with the already published literature by Ashraf [37]. Table 2 presents the statistical standards of skin friction at the lower disk for the case of hydrodynamic flows ($M = 0$) and MHD flows ($M = 1$). Skin friction increases with the decrease in the values of Reynolds number in both the cases (*i.e.*, $M = 1, M = 0$). From this observation we can conclude that in particular engineering applications of the problem under study, by selecting a

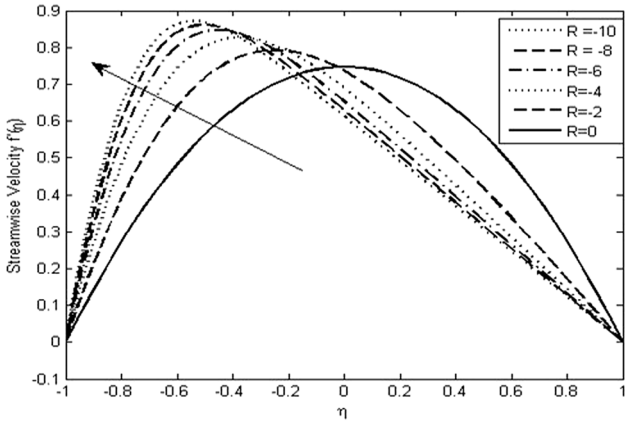

Figure 2: $f'(\eta)$ *versus* R.

Table 2: Values of skin friction $f''(-1)$ against altered values of R, when $M = 0$ and when $M = 1$

R	M	$f''(-1)$
0	0	1.5
−3		2.644
−6		3.529
−9		4.233
0	1	1.597
−3		2.653
−6		3.516
−9		4.213

suitable value of injection velocity at the porous disk, shear stress at nonporous/porous disk may be adjusted.

In the same manner, we discussed the effects of Reynolds number (R) on $f'(\eta)$ and $f(\eta)$ in Figures 2 and 3, respectively. On the other hand, the influence of Magnetic constraint (M) on streamwise velocity and normal velocity are discussed (Figures 4 and 5). Now, we probe the impact of Reynolds number R and graphical representation of streamwise and normal velocity profiles. Figure 2 displays the parabolic shape against $R = 0$. As the lower disk is porous, the profile irregularly moves in its direction subsequently growing in boundary layer width for the higher disk and declining for the bottom disk. Furthermore, the extreme velocity is lifted in the direction of the lower disk. We may additionally argue that an enhancement in the value of Reynolds number R intensifies these properties driving the main part of the flow toward the lower disk and for $R \to -\infty$, boundary layer thickness δ tends to zero. From Figure 2, it can be noted that streamwise velocity rises by increasing R. The behavior of normal velocity $f(\eta)$ against different values of Reynolds number $-10 \le R \le 0$ is shown in Figure 3. It can be perceived that for growth in R, normal velocity $f(\eta)$ increases throughout from the lower disk to upper disk. Numerical results of streamwise velocity and normal velocity have been presented graphically for the variation in M (Figures 4 and 5).

Figure 4 shows that the streamwise velocity profile decreases to close the lower disk by increasing the magnetic field parameter (M) and increases near the upper disk. Physically, the magnetic parameter is a measure of the magnetic field strength within the fluid. The Lorentz force appears due to the incorporation of the magnetic field in the fluid which opposes the fluid velocity. The magnetic effect near the porous disk decreases the stream velocity because of large Lorentz forces and the stream velocity increases toward the upper nonporous disk because of the small strength of Lorentz force. Figure 5 shows that velocity distribution declines with the rise in M because the magnetic field factor starts to slow down

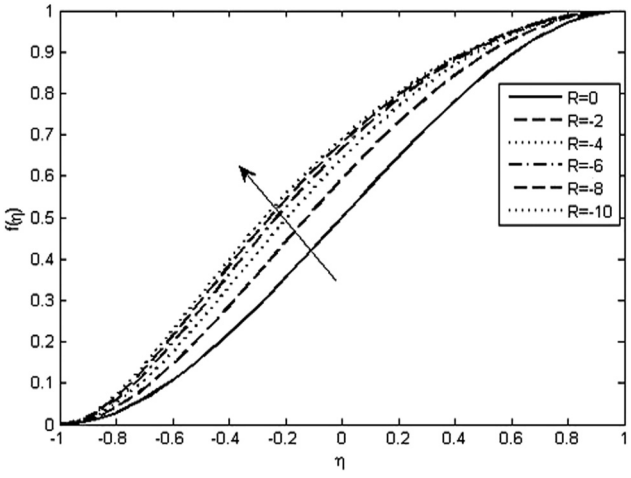

Figure 3: $f(\eta)$ *versus* R.

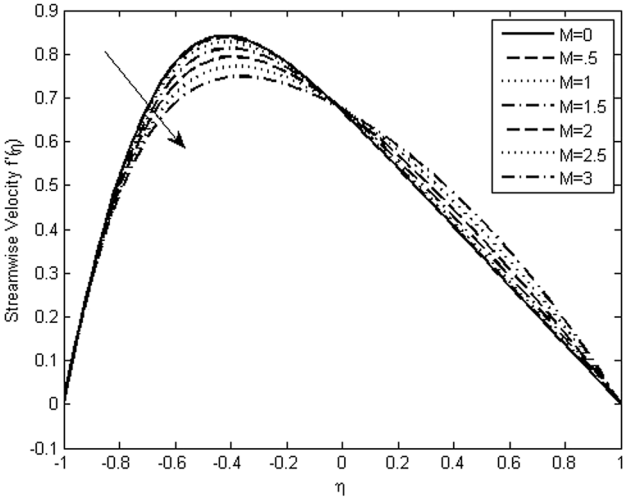

Figure 4: $f'(\eta)$ *versus* M.

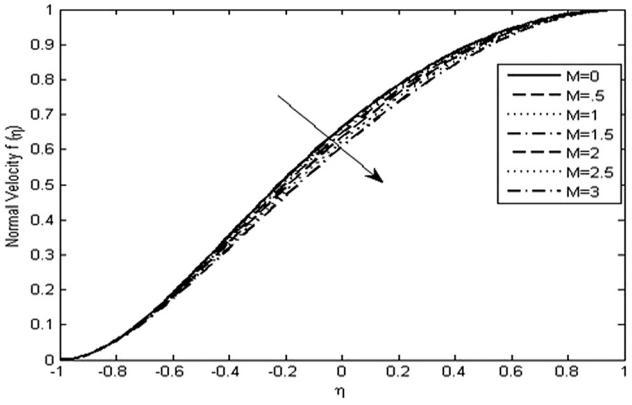

Figure 5: *f*(*η*) *versus M*.

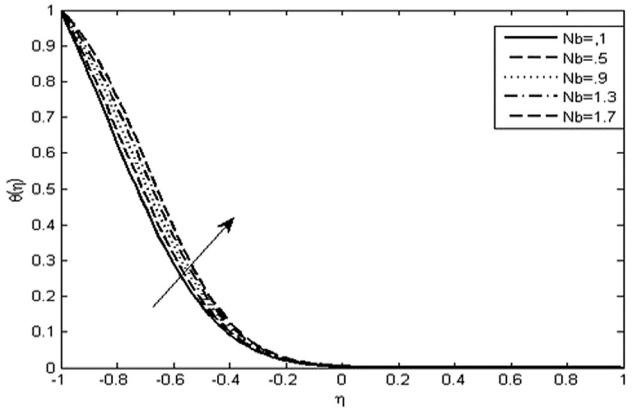

Figure 6: $\theta(\eta)$ *versus* Nb.

the velocity at all points of the flow field. It is due to an opposing force (Lorentz force) which tends to resist fluid flow. Also, with the increase in magnetic impact, boundary layer width decreases. The impacts of Brownian motion and thermophoresis parameters Nb and Nt on the temperature field $\theta(\eta)$ are discussed in the Figures 6 and 7, respectively.

The strength of Brownian motion and thermophoresis will be higher on the temperature field against Nb and Nt. The energy profile $\theta(\eta)$ significantly rises and the profile moves closer to the upper disk as Nb and Nt increase. The physics behind this is that by increasing the Brownian motion, the boundary layer wideness increases which increases the heat (because Brownian motion strength increases the temperature due to random movement).

Brownian motion and thermophoresis parameters (Nb, Nt) impact on the nanoparticles thermophoresis is illustrated in Figures 8 and 9, respectively. The concentration profile $\varphi(\eta)$ decreases with the increase in the value of the Brownian movement constraint. From

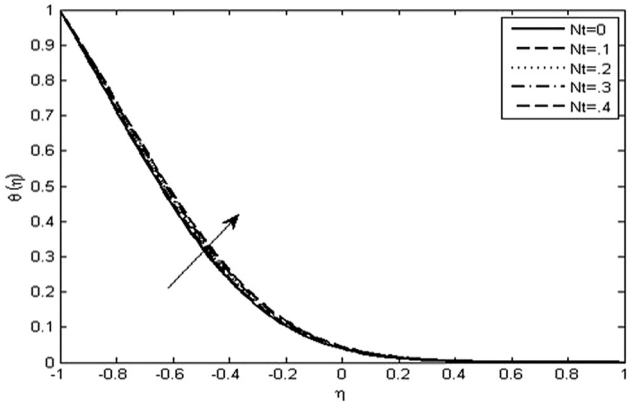

Figure 7: $\theta(\eta)$ *versus* Nt.

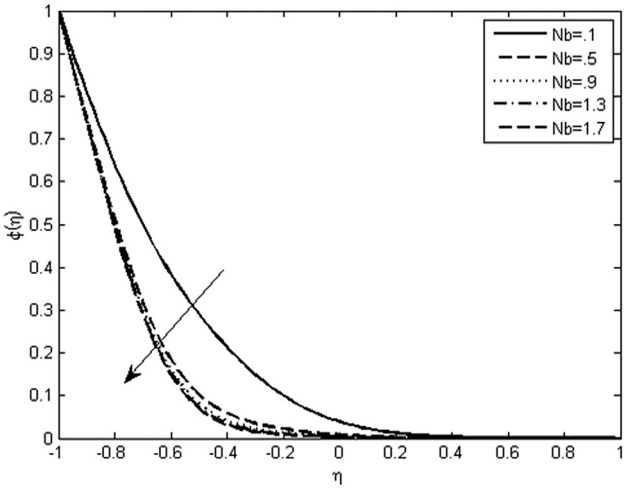

Figure 8: $\phi(\eta)$ *versus* Nb.

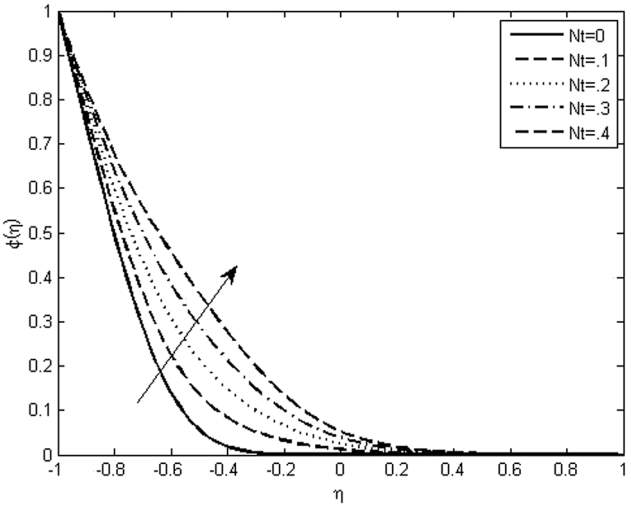

Figure 9: $\phi(\eta)$ *versus* Nt.

Eq. (12), it can be confirmed that the expression $\frac{1}{\mathrm{Nb}}$, shows direct correspondence with the nanoparticle concentration. Therefore, the concentration profile diminishes against the growth of Nb, while influence of Nt shows direct relation with $\varphi(\eta)$, thus the profile is increased. Physically, we can see that by increasing the thermophoretic effect due to the temperature gradient, a larger flux will be generated which in turn raises the concentration.

5 Conclusion

This article presented numerical simulations of nanofluid flow between a porous disk and a nonporous disk. We applied suitable similarity transformations to reduce the complex governing equations into a set of nonlinear ODEs. The numerical solutions are obtained by using the Lobatto method. Numerical simulations demonstrated the influence of physical parameters of interest, such as Reynolds number, magnetic factor, Brownian parameter, and thermophoresis parameter on normal velocity, streamwise velocity, temperature, and concentration profiles. Our results are in excellent agreement with the existing numerical literature results. For highly nonlinear differential equations, the Lobatto method is one of the most powerful, effective, and efficient tools to derive the solutions. The investigation of current work reveals that the heat and mass transfer along with flow phenomenon were influenced by physical factors. Additionally, this heat and mass transfer phenomenon provide useful information which can be utilized in paper production processes and in electronic devices. The main outcomes drawn from the above analysis are given as:

- The energy profile significantly rises for large values of Nb.
- Streamwise velocity enhanced against higher values of Reynolds number.
- Normal velocity decreases by increasing parameter M.
- $\theta'(-1)$ and $\varnothing'(-1)$ increases by increasing the values of thermophorsis (Nt).
- The concentration profile shows direct correspondence against thermophoretic effects.

Future work will focus on extending this study by selecting a suitable value of injection velocity at the porous disk shear stress at nonporous/porous disk. Moreover, we could consider different types of fluids such as hybrid nanoliquid, Williamson nanoliquid, Casson nanoliquid *etc*., with different numerical techniques.

Acknowledgments: The authors are thankful for the Taif University research supporting project number (TURSP-2020/304), Taif University, Saudi Arabia.

Funding information: This work was supported by Taif University research supporting project (Grant numbers. TURSP-2020/304).

Author contributions: conceptualization, validation, and formal analysis: Hammad Alotaibi; methodology, software, and investigation: Khuram Rafique; writing – original draft preparation and writing – review and editing: Hammad Alotaibi and Khuram Rafique. All authors have accepted responsibility for the entire content of this manuscript and approved its submission.

Conflict of interest: The authors state no conflict of interest.

References

[1] Choi SU, Eastman JA. Enhancing thermal conductivity of fluids with nanoparticles. Lemont, IL, USA: Argonne National Lab; 1995.
[2] Buongiorno J. Convective transport in nanofluids. J Heat Transf. 2006;128(3):240–50.
[3] Sheikholeslami M, Ellahi R, Hassan M, Soleimani S. A study of natural convection heat transfer in a nanofluid filled enclosure with elliptic inner cylinder. Int J Numer Methods Heat Fluid Flow. 2014;24(8):1906–27.
[4] Dogonchi AS, Chamkha AJ, Seyyedi SM, Ganji DD. Radiative nanofluid flow and heat transfer between parallel disks with penetrable and stretchable walls considering Cattaneo–Christov heat flux model. Heat Transfer – Asian Res. 2018;47(5):735–53.
[5] Mohyud-Din ST, Zaidi ZA, Khan U, Ahmed N. On heat and mass transfer analysis for the flow of a nanofluid between rotating parallel plates. Aerosp Sci Technol. 2015;46:514–22.
[6] Sheikholeslami M, Abelman S. Two-phase simulation of nanofluid flow and heat transfer in an annulus in the presence of an axial magnetic field. IEEE Trans Nanotechnol. 2015;14(3):561–9.
[7] Hosseinzadeh K, Alizadeh M, Ganji DD. Hydrothermal analysis on MHD squeezing nanofluid flow in parallel plates by analytical method. Int J Mech Mater Eng. 2018;13(1):4.
[8] Rafique K, Anwar ML, Misiran M, Khan I, Baleanu D, Nisar KS, et al. Hydromagnetic flow of micropolar nanofluid. Symmetry. 2020;12(2):251.
[9] Noor NF, Haq RU, Nadeem S, Hashim I. Mixed convection stagnation flow of a micropolar nanofluid along a vertically stretching surface with slip effects. Meccanica. 2015;50(8):2007–22.

[10] Mabood F, Khan WA, Ismail AM. MHD boundary layer flow and heat transfer of nanofluids over a nonlinear stretching sheet: a numerical study. J Magnetism Magnetic Mater. 2015;374:569–76.
[11] Azimi M, Riazi R. Analytical simulation of mixed convection between two parallel plates in presence of time dependent magnetic field. Indian J Pure Appl Phys. 2016;54:327–32.
[12] Makinde OD, Mahanthesh B, Gireesha BJ, Shashikumar NS, Monaledi RL, Tshehla MS. MHD nanofluid flow past a rotating disk with thermal radiation in the presence of aluminum and titanium alloy nanoparticles. Defect Diffus Forum. 2018;384:69–79.
[13] Turkyilmazoglu M. Exact solutions for the incompressible viscous magnetohydrodynamic fluid of a rotating disk flow. Int J Nonlinear Mech. 2011;46:306–11.
[14] Rafique K, Anwar MI, Misiran M, Khan I, Seikh AH, Sherif ES, et al. Brownian motion and thermophoretic diffusion effects on micropolar type nanofluid flow with Soret and Dufour impacts over an inclined sheet: Keller-box simulations. Energies. 2019;12(21):4191.
[15] Rafique K, Anwar ML, Misiran M, Khan L, Seikh AH, Sherif ES, et al. Keller-Box simulation for the Buongiorno mathematical model of micropolar nanofluid flow over a nonlinear inclined surface. Processes. 2019;7(12):926.
[16] Iqbal MS, Ghaffari A, Riaz A, Mustafa I, Raza M. Nanofluid transport through a complex wavy geometry with magnetic and permeability effects. Inventions. 2021;7(1):7.
[17] Iqbal MS, Mustafa I, Ghaffari A. A computational analysis of dissipation effects on the hydromagnetic convective flow of hybrid nanofluids along a vertical wavy surface. Heat Transf. 2021;50(8):8035–51.
[18] Elcrat AR. On the radial flow of a viscous fluid between porous disks. Arch Ration Mech Anal. 1976;61(1):91–6.
[19] Ibrahim FN. Unsteady flow between two rotating discs with heat transfer. J Phys D: Appl Phys. 1991;24(8):1293–9.
[20] Vajravelu K, Prasad KV, Ng CO, Vaidya H. MHD squeeze flow and heat transfer of a nanofluid between parallel disks with variable fluid properties and transpiration. Int J Mech Mater Eng. 2017;12(1):1–14.
[21] Bhatta DP, Mishra SR, Dash JK. Unsteady squeezing flow of water-based nanofluid between two parallel disks with slip effects: Analytical approach. Heat Transfer – Asian Res. 2019;48(5):1575–94.
[22] Hayat T, Abbas T, Ayub M, Muhammad T, Alsaedi A. On squeezed flow of Jeffrey nanofluid between two parallel disks. Appl Sci. 2016;6(11):346.
[23] Sobamowo MG, Akinshilo AT, Yinusa A. Thermo-Magneto-Solutal Squeezing Flow of Nanofluid between Two Parallel Disks Embedded in a Porous Medium: Effects of Nanoparticle Geometry. Slip Temp Jump Cond Model Simul Eng. 2018;2018:1–18.
[24] Ghaffari A, Muhammad T, Mustafa I. Heat transfer enhancement in a power-law nanofluid flow between two rotating stretchable disks. Pramana. 2022;96(1):1–11.
[25] Aziz A, Alsaedi A, Muhammad T, Hayat T. Numerical study for heat generation/absorption in flow of nanofluid by a rotating disk. Results Phys. 2018;8:785–92.
[26] Elakkiyapriya T, Anjali SP. Buongiorno model with revised boundary conditions for hydromagnetic forced convective nanofluid flow past a rotating porous disk. Int J Mathematics Trends Technol (IJMTT). 2018;55(3):212–22. ISSN:2231-5373.
[27] Hatami M, Jing D, Yousif MA. Three-dimensional analysis of condensation nanofluid film on an inclined rotating disk by efficient analytical methods. Arab J Basic Appl Sci. 2018;25(1):28–37.
[28] Yin C, Zheng L, Zhang C, Zhang X. Flow and heat transfer of nanofluids over a rotating disk with uniform stretching rate in the radial direction. Propuls Power Res. 2017;6(1):25–30.
[29] Rafique K, Alotaibi H, Nofal TA, Anwar MI, Misiran M, Khan I. Numerical solutions of micropolar nanofluid over an inclined surface using Keller Box analysis. J Math. 2020;2020:1–13.
[30] Alotaibi H, Althubiti S, Eid MR, Mahny KL. Numerical treatment of MHD flow of casson nanofluid *via* convectively heated nonlinear extending surface with viscous dissipation and suction/injection effects. Computers Mater Continua. 2020;66(1):229–45.
[31] Alotaibi H, Eid MR. Thermal analysis of 3D electromagnetic radiative nanofluid flow with suction/blowing: Darcy–Forchheimer scheme. Micromachines. 2021;11:1395(12). doi: 10.3390/mi12111395.
[32] Alotaibi H, Rafique K. Numerical analysis of micro-rotation effect on nanofluid flow for vertical Riga plate. Crystals. 2021;11:1315. doi: 10.3390/cryst11111315.
[33] Khan M, Huda NU, Hamid A. Non-linear radiative heat transfer analysis during the flow of Carreau nanofluid due to wedge-geometry: a revised model. Int J Heat Mass Transf. 2019;131:1022–103.
[34] Basir MF, Hafidzuddin ME, Naganthran K, Chaharborj SS, Kasihmuddin MS, Nazar R. Stability analysis of unsteady stagnation-point gyrotactic bioconvection flow and heat transfer towards the moving sheet in a nanofluid. Chin J Phys. 2020;65:538–53.
[35] Rafique K, Alotaibi H. Numerical simulation of Williamson nanofluid flow over an inclined surface: Keller Box analysis. Appl Sci. 2021;11(23):11523.
[36] Hamid A, Hashim, Khan M. Heat generation/absorption and velocity slip effects on unsteady axisymmetric flow of Williamson magneto-nanofluid. Mod Phys Lett B. 2019;33(34):1950432.
[37] Ashraf M, Wehgal AR. MHD flow and heat transfer of micropolar fluid between two porous disks. Appl Math Mech. 2012;33(1):51–64.
[38] Ashraf M, Kamal MA, Syed KS. Numerical simulation of flow of a micropolar fluid between a porous disk and a non-porous disk. Appl Math Model. 2009;33(4):1933–43.
[39] Von Kármán T. Über laminare und turbulent reibung Z. angew. Math und Mech. 1921;1:233–52.
[40] Elkouh AF. Laminar flow between rotating porous disks. J Eng Mech Div. 1968;94(4):919–30.